# Full-scale testing and platform stabilization of a scanning lidar system for planetary landing

Andrew C. M. Allen[*a], Christopher Langley[a], Raja Mukherji[a], Manny Nimelman[a],
Jean de Lafontaine[b], David Neveu[b], Jeffrey W. Tripp[c]

[a]MDA Space Missions, 9445 Airport Rd., Brampton, Ont., Canada L6S 4J3;
[b]NGC Aerospace, 202 – 1650 rue King Ouest, Sherbrooke, Que., Canada, J1J 2C3;
[c]Optech, 300 Interchange Way, Vaughan, Ont., Canada L4K 5Z8

## ABSTRACT

In August 2007, the engineering model of the Rendezvous Lidar System (RLS) was tested at the Sensor Test Range Facility that has been developed at NASA Langley Research Center for the calibration and characterization of 3-D imaging sensors. The three-dimensional test pattern used in this characterization is suitable for an empirical verification of the resolving capability of a lidar for both mid-range terminal rendezvous and hazard avoidance landing. The results of the RLS lidar measurements are reported and compared with image frames generated by a lidar simulator with an Effective Instantaneous Field of View (EIFOV) consistent with the actual scanning time-of-flight lidar specifications. These full-scale tests demonstrated the resolving capability of the lidar under static testing conditions. In landing operations, even though the lidar has a very short exposure time on a per-pulse basis, the dynamic motion of a lander spacecraft with respect to the landing site will cause pulse-to-pulse imaging distortion. MDA, Optech, and NGC Aerospace have teamed together to resolve this issue using motion compensation (platform stabilization) and motion correction (platform residual correction) techniques. Platform stabilization permits images with homogenous density to be generated so that no safe landing sites will be missed; platform residual errors that are not prevented by this stabilization are then corrected in the measurement data prior to map generation. The results of recent developments in platform stabilization and motion correction are reported and discussed in the context of total imaging error budget.

**Keywords:** landing, descent, lander, lidar, ladar, sensor, hazard avoidance, navigation, guidance, GNC

## 1. INTRODUCTION

Previous planetary exploration missions requiring low touchdown rates have maximized the likelihood of success by selecting landing areas with relatively flat, hazard-free terrain over the uncertainty ellipse of the landing spacecraft. Future exploration missions requiring soft landing on the lunar or Martian surfaces will seek to land in particular regions of interest, either for targeted scientific study, identification of *in situ* resources, or establishment of a manned presence. Many of the proposed regions of interest have terrains that do not meet the flatness and hazard-free criteria used in prior mission planning. Technologies that permit the detection of safe landing sites during descent will be compulsory for these missions.

As early as the end of 2008, the Lunar Reconnaissance Orbiter spacecraft will be orbiting the moon with the capability of performing mapping and hazard detection at a 2-meter scale [2]; however, landers will likely need to avoid hazards at the 30 to 50 centimeter scale [3][1]. Consequently, there is a need for a landing sensor system which can measure the terrain with sufficient resolution to provide an assessment of the terrain in terms of its local slope, roughness, and reachability. The location of the site with the lowest combined slope, hazard distribution, and propellant cost to divert is then used by the lander's guidance function to specify the terminal location of its landing trajectory.

This paper presents the results of continued development of the Lidar-based Autonomous Planetary Landing System (LAPS). Section 2 describes the advantages of using a lidar-based system for planetary landing. The key role played by *a priori* and *a posteriori* motion compensation is also highlighted. The operational concept of a LAPS-equipped descent scenario is detailed in Section 3. The results of full-scale tests performed at NASA Langley are presented and compared with the performance model in Section 4. Conclusions and future development directions are discussed in Section 5.

---

[*] andrew.allen@mdacorporation.com; phone 1-905-790-2800 ext. 4780; fax 1-905-790-4400; http://sm.mdacorporation.com/

## 2. SCANNING TIME-OF-FLIGHT LIDAR

The Lidar-based Autonomous Planetary landing System (LAPS), as its name implies, is intended to be a guidance, navigation, and control (GNC) system for planetary landers [5][6][7][8][9]. The primary sensor in the first-generation system is a time-of-flight scanning lidar unit which has several advantages for planetary landing:

- Operational range: The scanning lidar has an operational range from several kilometers (depending on the reflectivity and size of the target object) down to a few meters with a credible peak power requirement, unlike a pure flash lidar system.

- Illumination invariance: The lidar is an active illuminator with performance invariant to ambient lighting conditions, unlike a camera-based system. LAPS can therefore be applied to landing on the dark side of planetary bodies, or within the basins of permanently shadowed craters. The pulse duration, and therefore the exposure time per measurement, is approximately 1 nanosecond.

- Feature invariance: The lidar works equally well on terrain which does or does not contain any visual features, or is not illuminated (e.g., landings in polar regions), unlike an optical correlator system [10].

- Imaging capability: The lidar can create a high-resolution three-dimensional image of the surface, unlike a radar-based system [11].

The sensor measures the time of flight of a short duration (~1 ns) laser pulse which reflects off of a surface and returns to the sensor aperture. Using the speed of light, the time of flight is converted into the path length of the laser pulse, and hence, the range from the sensor to the surface can be measured. By steering the beam, the lidar is able to "paint" an object with laser pulses at high rate (~10 kHz) to create a three-dimensional image of the object.

The first-generation LAPS hardware architecture consists of three items: the Optical Head Unit (OHU), the Avionics Unit (AU), and the cable harnesses connecting them. This architecture follows that used in the current space lidar design, shown in Figure 1.
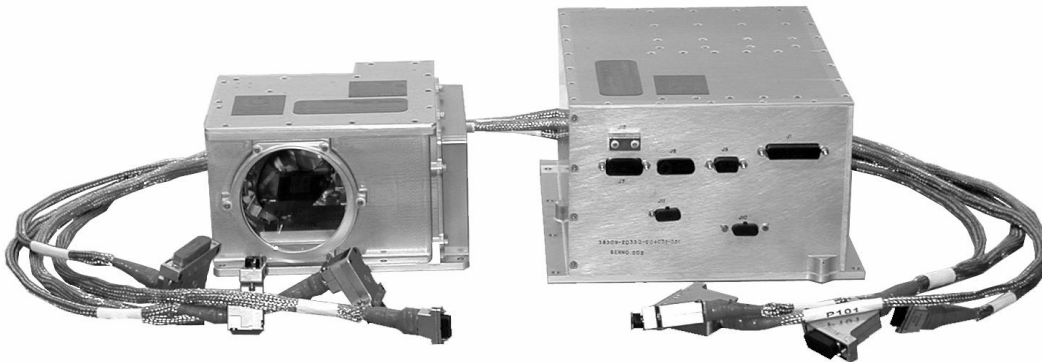


**Figure 1: XSS-11 Lidar OHU & AU**

The XSS-11 lidar was launched in April 2005 and operated successfully throughout the spacecraft's mission life. In addition to a sensor with this heritage, LAPS includes onboard GNC software to perform state estimation, generation of guidance references, and generation of feedback control signals which can be used to drive the lander actuators.

### 2.1 Motion compensation requirements

Unlike a camera, which acquires all of its data in parallel, the lidar sequentially acquires scan points as the beam is steered over the object. The time required to complete a scan is therefore a major design driver in the use of lidar in a planetary landing system. The lidar scanning mirror requires some time to trace out the scan pattern and to acquire an image. However, during a planetary descent, the lidar itself is moving with respect to the terrain being scanned. Motion of the sensor frame while the scan is occurring has the following distortion effects:

- **Scan pattern distortion**: The lander motion distorts the scan pattern on the terrain. This distortion degrades the spatial sampling and affects the ability to detect hazards.

- **Data distortion:** Since each point is measured with respect to the lidar frame, the sequential data will be distorted by the landing vehicle motion.

These distortions can be strongly counteracted using a *motion compensation* scheme. Firstly, the scan pattern distortion can be removed at the mirror level using *a priori* compensation (also called *platform stabilization*, as it makes the lidar behave, in effect, like a stable platform). This ensures that the correct region of the terrain is scanned and re-scanned with the correct spatial sampling. Secondly, the sequential data distortion can be removed as the laser pulses return using *a posteriori* compensation (also called *post-processing motion correction*). This enables all of the data to be expressed in a frame that is stationary with respect to the terrain. Both schemes must be applied to image the terrain within the error budget for detecting 30-centimeter hazards.

The motion correction code takes lidar scan data (in the form of time-stamped point clouds) and applies a time-varying transformation based on the spacecraft state telemetry to express all of the measurements in the same frame. This correction is a necessary stage before the data is passed to the cost mapping and safe site selection algorithm. The function of platform stabilization is to ensure an even spatial distribution of lidar samples on the ground, given that the lidar itself is in motion. Based upon an estimate of the lander motion, a scan correction signal is applied to the lidar mirror angles.
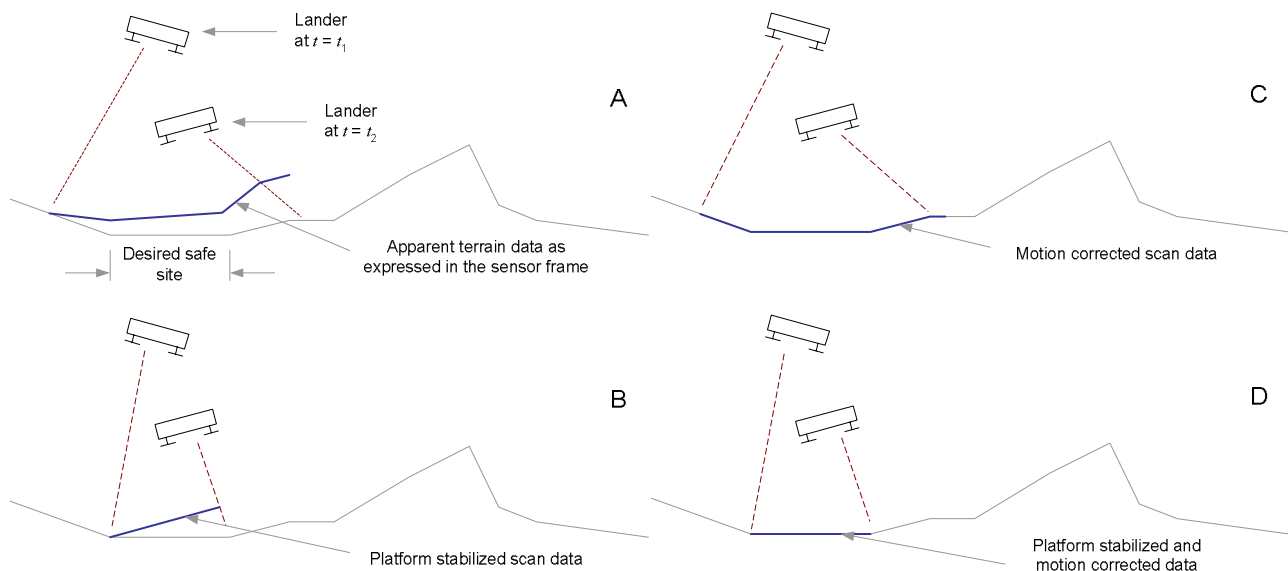


**Figure 2: Two-dimensional example illustrating the need for both platform stabilization and post processing motion correction. The lidar beam (dashed line) scans from left to right as the lander descends.**

To illustrate this effect, an exaggerated case is shown in two dimensions in Figure 2. The lidar acquires data while it is descending, translating laterally, and while rotating. The acquired data, as expressed in the lidar frame, is distorted in two ways: it covers more of the terrain than desired, and appears to slant upward (Figure 2A) due to the diminishing altitude throughout the scan. If the same descent and scan is performed using only platform stabilization, the correct region of the terrain will be scanned, but the data will be distorted (Figure 2B). Conversely, if only post-processing motion correction is applied, the data will all be expressed in a meaningful frame, but the spatial sampling of the desired landing site will be less uniform than desired and will cover the wrong landing area (Figure 2C). Only by applying both techniques will the lidar acquire and report the image data correctly (Figure 2D).

## 2.2 Testing of platform stabilization and motion correction

Error analysis becomes critical when motion compensation is considered. The ability to correctly image a landing site via sequential sampling is limited by the ability of the sensor system to compensate for the motion of the spacecraft. By extension, the effectiveness of motion compensation depends on the accuracy of the dynamic state knowledge of the lander. Contributions to the imaging error budget of the lidar arise from linear velocity and angular rate knowledge errors, latency in the state estimates, range resolution and beam divergence, and mirror pointing resolution.

When applied to a vehicle in motion, the platform stabilization alters the scan pattern execution to provide an image ideally equivalent to one produced by a static sensor. Figure 3 shows tests of the platform stabilization implementation

that demonstrates how the motion of the fine steering mirror cancels out the effects of bearing drifts (or the equivalent lateral drifts) resulting in a stabilized pseudo-static image. The initial loop in the scans is the result of starting the scans with the mirror pointing along the optical center of the sensor; in operation, the scans will run continuously with no start-up transients. In all testing, the residual errors from both the platform stabilization and the motion correction were well within the operational requirements of the first-generation scanning lidar landing sensor.
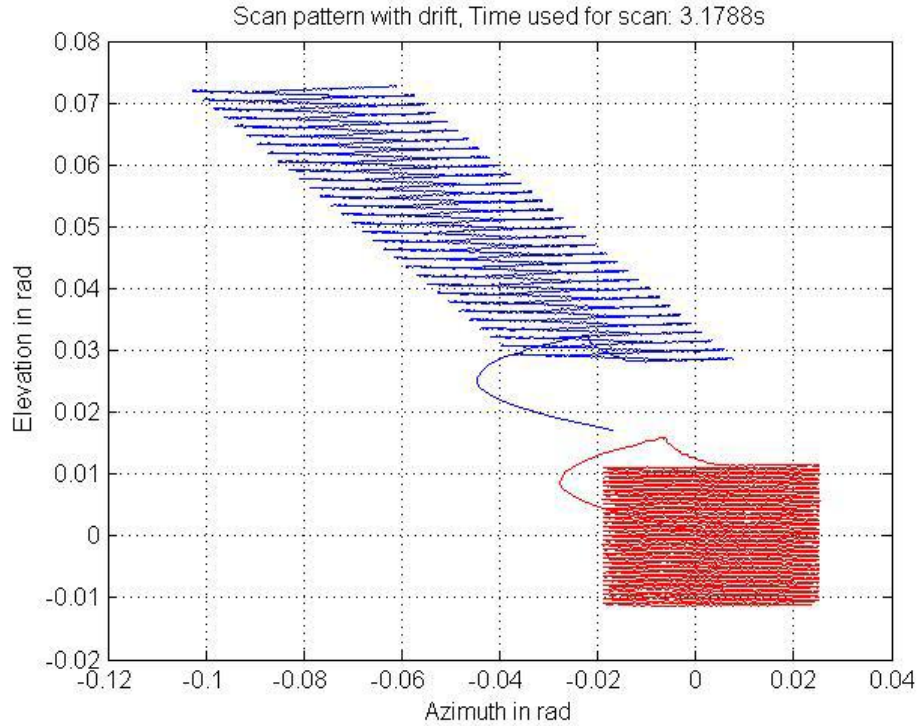


**Figure 3: Platform-stabilized scan results azimuth drift of -0.022 rad/sec and elevation drift of 0.022 rad/sec red: fixed frame scan. blue: stabilized scan for moving frame. (with steady-state offset added for clarity)**

## 3. THE LAPS OPERATIONAL CONCEPT

After establishing the practicality of stabilizing a lidar imager to provide sequential data collection on a descending lander, we return to the operations concept to verify that the sufficient image size and resolution can be obtained with this sensor system concept. The LAPS operations have been described in detail in [12]; a summary is provided below.

### 3.1 Definition of a safe landing site

The definition of a safe landing site is strongly influenced by the type of lander, its size, structure and design. The definition summarized in Table 1 is based on inputs from [3] and [12].

**Table 1: Definition of a safe landing site**

| Parameter | Value | Comment |
|---|---|---|
| Area of interest | $100 \times 100$ m$^2$ | The lander will land within this area. |
| Lander size | Ø 2.5 m | Viking-sized lander |
| Size of safe landing site | Ø 5 m | Twice the size of the lander |
| Maximum local slope | 15° | Viking & Phoenix reqm't over the extent of the landing site |
| Maximum sampling step for slope determination | 1 m | Sufficient for measuring local slope within the landing site |
| Maximum allowed boulder size | 30 cm | Phoenix lander requirement |
| Minimum resolution for roughness determination | 10 cm | Sufficient for measuring roughness within the landing site |

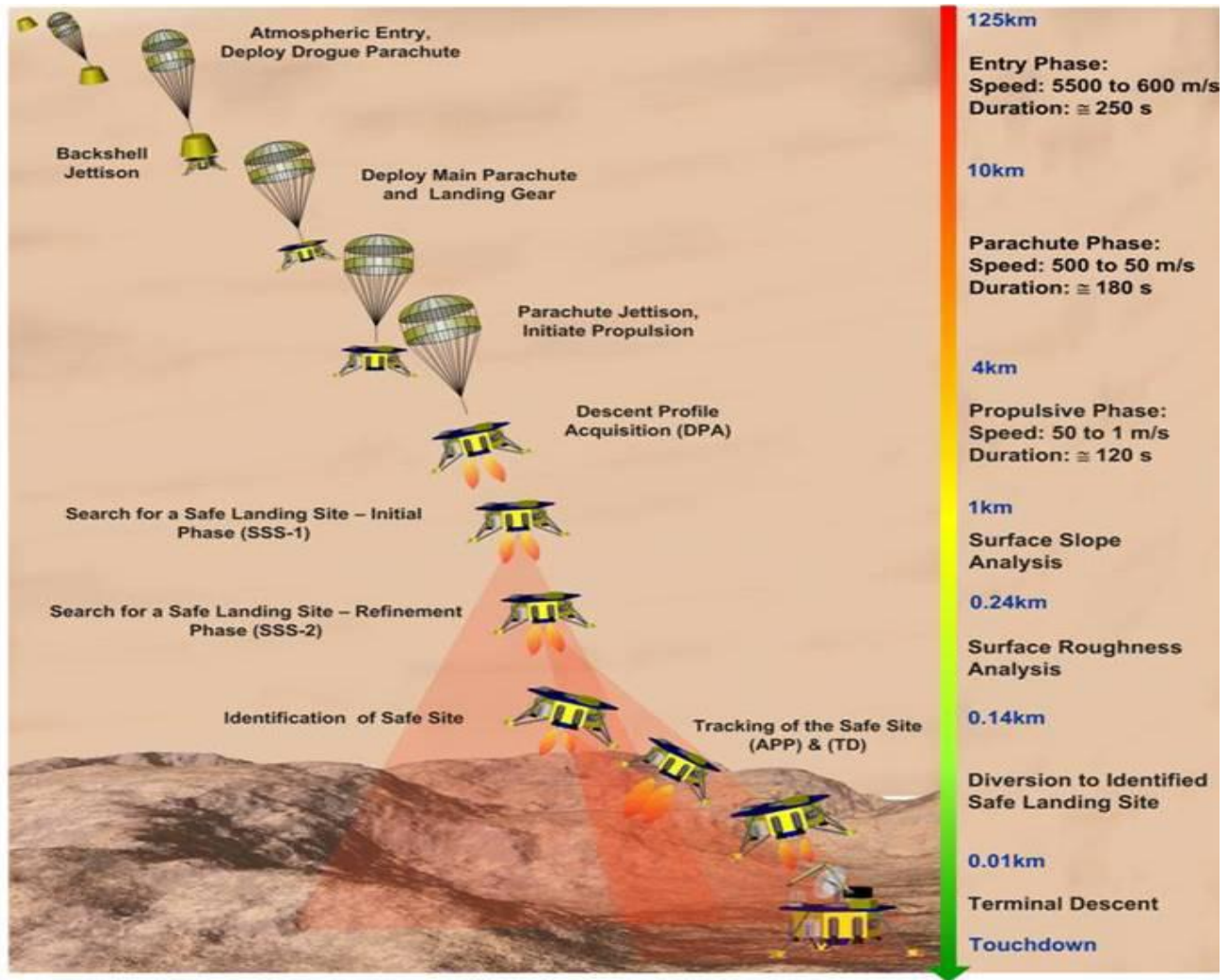## 3.2 Design reference mission



**Figure 4: Illustration of the LAPS operational stages [Courtesy NGC Aerospace]**

Given the definition of a safe landing site, the hazard avoidance landing sensor must determine safe sites sufficiently in advance of touchdown for the lander to be redirected to the best of the safe sites. In this context it fulfils the role of a guidance sensor. With the addition of terrain-relative navigation (currently in development [14]), the sensor can be used for pinpoint landing and as a low-bandwidth closed-loop navigation input. In order to more clearly define the LAPS concept, it is useful to subdivide the descent phase of the operation stages as shown in Figure 4. The LAPS system is used primarily in the Safe Site Search stages as described below:

**Safe-Site Search (SSS-1) – Slope Detection:** This mode has an objective to search for and identify a number of safe site candidates (e.g., five) in a landing area of a certain size (e.g., 100 m × 100 m). The potential safe sites are identified by assessing the local slope, which is found by placing a specified density of points within a lander-sized region (e.g., 25 points per 5 m × 5 m area) and fitting a mean plane through the measured points after excluding returns from large out-of-plane objects like outcroppings and chasms. A cost map can be generated based upon this local slope and upon the divert propellant required to reach a given site. The landing area may be scanned several times (e.g., three times with a voting scheme) for reliability. This mode ends when the safe site candidates have been identified and the lidar has sufficient spatial resolution to detect roughness hazards.

**Safe Site Search (SSS-2) – Hazard Detection:** This operational stage starts at the altitude where the lidar resolution permits roughness assessment, and ends at the altitude where the lander must commit to a landing at a selected site

(either due to its propellant budget or due to candidate safe sites leaving the lidar field of view). This mode has an objective to identify any hazards within any of the candidate safe regions based on the roughness assessment, which is performed by placing a certain density of points within a hazard-sized region (e.g., 10 points per $30 \times 30$ cm area). Cost maps can be generated based on the local slope, roughness, and upon the divert propellant required to reach a given site.

In both safe site search stages and in the terminal tracking of the chosen safe site, both *a priori* and *a posteriori* motion compensation must be used in order to produce meaningful scan data (as described in Section 2.1).

A natural tradeoff exists when defining the altitude and duration budgets for the stages of the descent. Designing the descent for minimum propellant results in a fast descent, but with less certainty about the safety of the landing site. Slowing down the SSS-1 and SSS-2 stages to allow the sensor more time to generate images of the site increases the certainty of safety, but incurs additional propellant usage. The LAPS design reference mission seeks to find a balanced design point in the tradeoff. Obviously, to make the lidar-assisted safe landing an attractive option, the goal is to alter the nominal descent trajectory as little as possible thereby maintaining the maximal payload fraction in the lander. In that way, the design reference mission has the smallest possible impact on landing propellant usage while still maintaining credible operating conditions for the lidar.
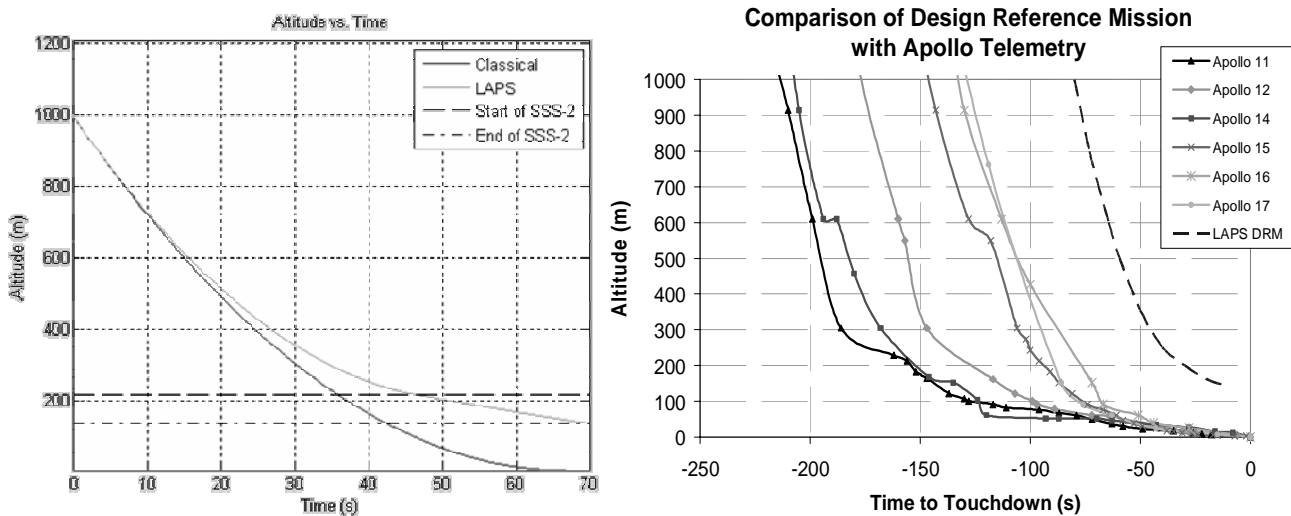


**Figure 5: (left) Altitude as a function of time for the reference descent profile**
**(right) Comparison of the LAPS design reference mission with Apollo telemetry**

Details of the design of the reference descent can be found in [12]. Here it is sufficient to note that the time to perform the necessary scans and the effective spatial resolution of the lidar are used to determine the altitude ranges for SSS-1 and SSS-2. A piecewise-continuous form of the gravity turn guidance law [7] is used to generate the descent, shown in Figure 5(left). Note that even though the LAPS trajectory is slower than the nominal gravity turn, it is still significantly faster than the Apollo moon landing trajectories [15], as shown in Figure 5(right). The Apollo landings are significant because they represent the only prior hazard avoidance landing missions, albeit with a human in the loop.

**LAPS flight baseline**

**Table 2 – Specifications for the flight lidar**

| Parameter | Flight Specification | XSS-11 Specification | Lab (ILRIS) Specification |
|---|---|---|---|
| Mirror Acceleration | 920 rad/s$^2$ | 230 rad/s$^2$ | > 145 rad/s$^2$ |
| Controller Bandwidth | 240 Hz | 80 Hz | 60 Hz |
| Controller Damping | 0.5 | 0.3 | 0.3 |
| PRF | 10 kHz | 10 kHz | 2 kHz |
| FOV | +/- 20° | +/- 10° | +/- 20° |
| Range Resolution | 2 cm, 3 σ | 5 cm, 3 σ | 1 cm, 3 σ |
| Beam Divergence | 170 μrad | 500 μrad | 170 μrad |

The flight lidar for use as a safe landing sensor has not yet been built and tested; however, a development path has been established for a first-generation landing lidar based on the XSS-11 flight lidar heritage. Table 2 compares the flight specification with the XSS-11 lidar and the terrestrial ILRIS-3D system used in the LAPS Development Test Facility [16]. The major areas of improvement are the mirror acceleration, mirror controller bandwidth, and the range and bearing resolution. The improved performance specifications have been used to derive the timing and imaging error budgets, and thereby show that the design reference mission that has been established is credible.

## 4. STATIC TESTING USING THE ALHAT TARGET

In August 2007, the LAPS team had the opportunity to perform static tests of the lidar unit in a landing sensor capacity using the Autonomous Precision Landing and Hazard Detection Avoidance Technology (ALHAT) target located at the NASA Langley Research Center [17]. The ALHAT Sensor Test Range (STR) consists of a three-dimensional calibrated test target located 250 meters from the sensor platform. The target board uses variations in reflectivity, slope, width, and depth of its features (see Figure 6) in order to test the resolution and sensitivity of candidate hazard avoidance sensors. The test target is, in effect, a meticulously designed test pattern to measure the spatial resolution of three-dimensional sensors at spatial frequencies and ranges consistent with the requirements for planetary soft landing. Further details of the facility can be found in [17].
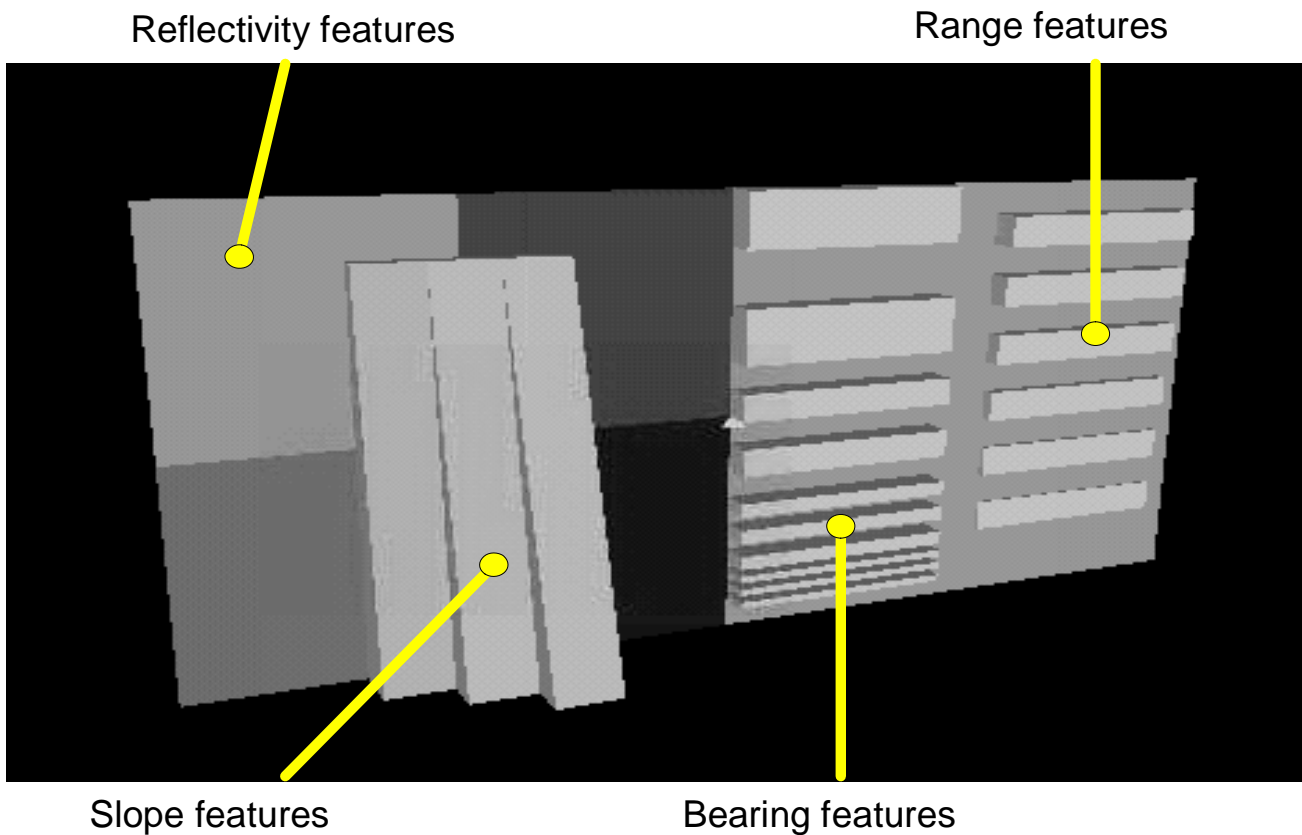


**Figure 6: 3D visualization of the ALHAT target board detailed in [17]**

The tests on the ALHAT target were performed using both the Engineering Model (EM) of the XSS-11 lidar and the ILRIS-3D terrestrial lidar. A sample dense scan of the target board using an engineering model of the XSS-11 lidar is shown in Figure 7. Note that these tests were conducted with the sensors mounted on a static test stand and that no platform stabilization or motion correction was in use at the time of imaging. Future testing, with a platform-stabilized and motion-corrected scanning lidar sensor mounted on a representative dynamic platform, will be required to validate

that this demonstrated static spatial resolution is not degraded below the level required in the operations concept for safe site imaging.
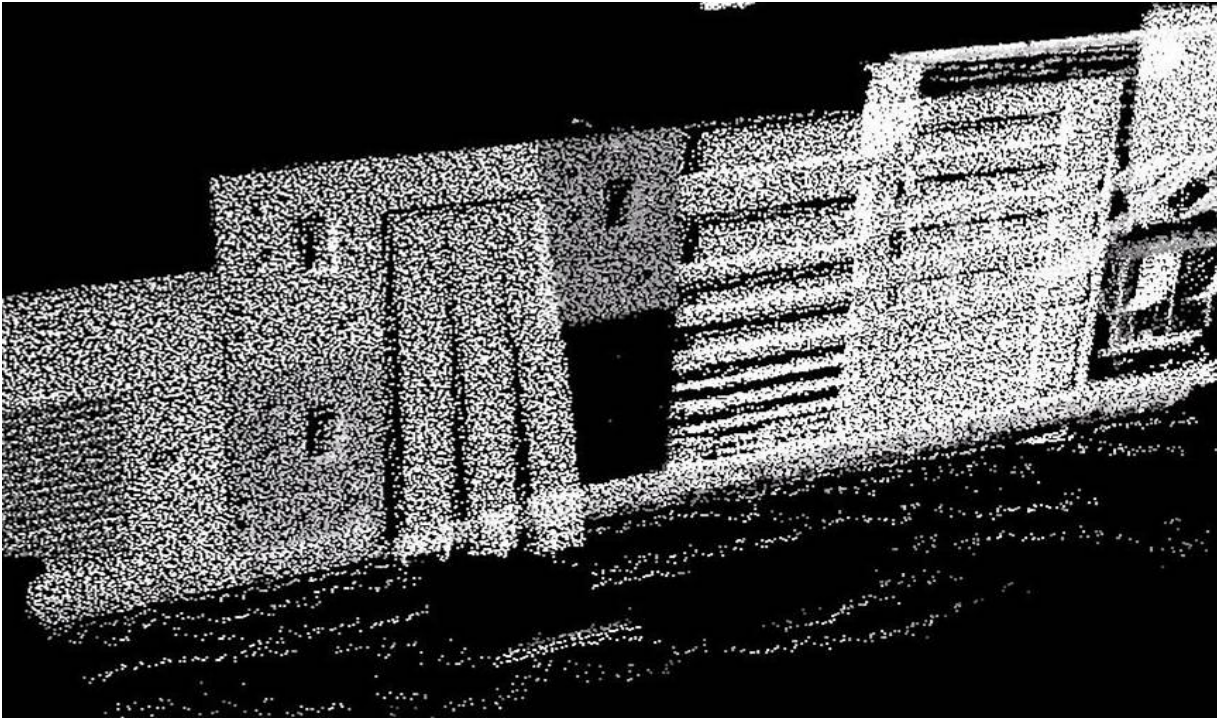


**Figure 7: 3D points acquired by densely scanning the ALHAT target board with the XSS-11 EM lidar from 250 m**

The XSS-11 lidar was designed for orbital rendezvous and proximity operations rather than planetary landing, and the unit does not have either the acceleration or the imaging performance of the LAPS baseline (see Table 2). However, the testpattern data was used to validate a performance model of the XSS-11 EM unit, which was based on the Average Modulation Transfer Function (AMTF) of the optical system [18]. The AMTF describes the average sensitivity of the lidar to different spatial frequencies, given a commanded scan density and beam spot size at the target.
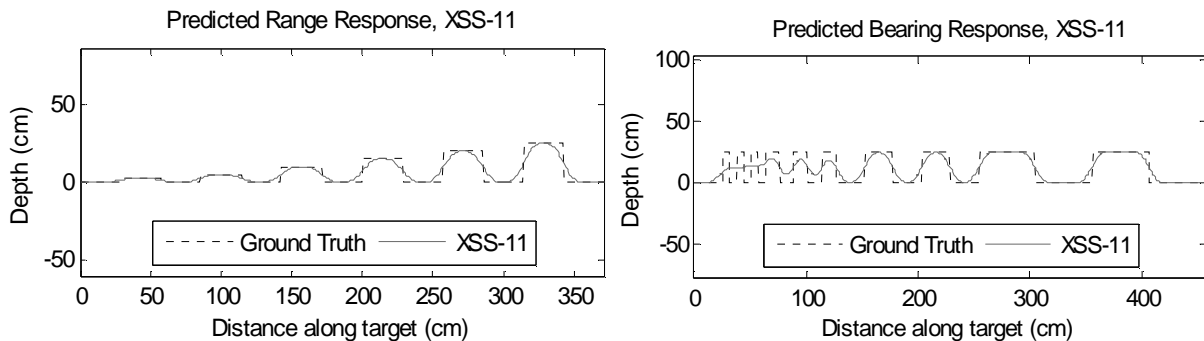


**Figure 8: Predicted average response of the RLS to the ALHAT testpattern. Left: range Right: bearing**
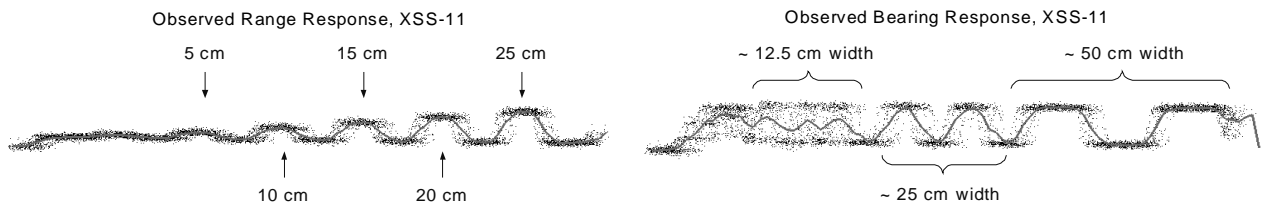


**Figure 9: Observed raw points (black) and average signal (magenta). Left: range Right: bearing**

Using the ALHAT target board geometry as an input to the performance model, the average response of the XSS-11 EM unit was predicted (Figure 8). The experimental data was processed by extracting the range and bearing signals from a sparse scan (Figure 10) and averaging the depth values as a function of the distance along the target board (Figure 9). Note the close agreement of the predicted edge distortions and in the attenuation of the 12.5 cm width features; as an aside, this implicitly validate the concept of an Effective Instantaneous Field of View (EIFOV) which is a useful angular resolution performance term [18] that can be readily incorporated into a pulse-by-pulse lidar simulator rather than the gross AMTF image-level metric.

With this degree of model validation, the LAPS baseline parameters were then used to predict the performance of the LAPS sensor under these test conditions (Figure 11). Note that the edges are less distorted and that the LAPS sensor can resolve the 12.5 cm features with little attenuation at 250 meters.
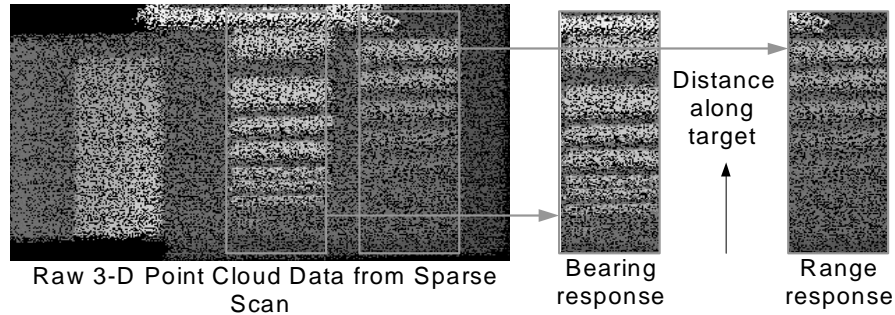


Figure 10: Extraction and range (blue) and bearing (green) response data from a sparse scan
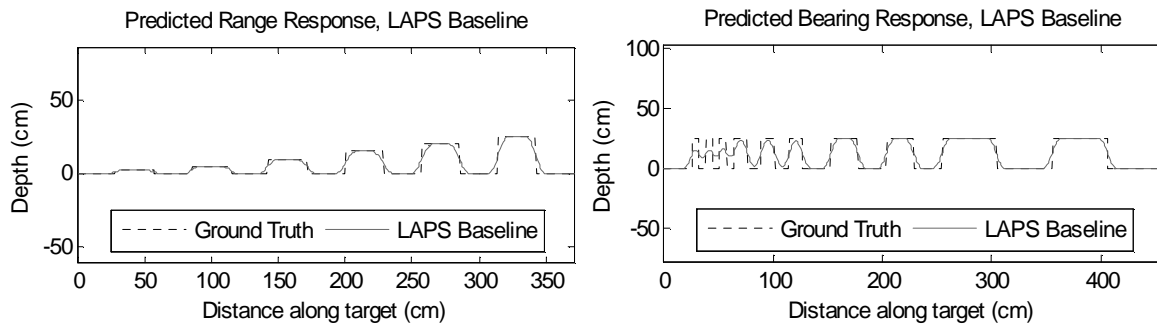


Figure 11: Predicted performance of the LAPS lidar sensor under the test conditions. Left: range Right: bearing

## 5. CONCLUSIONS AND FUTURE WORK

The LAPS research and development projects have established a credible design reference mission for a first-generation scanning lidar-based hazard avoidance landing system. The required lidar performance was specified, using a realizable development path from existing terrestrial and flight heritage.

Full-scale static tests of the XSS-11 Engineering Model rendezvous lidar using the ALHAT target have been used to validate the LAPS sensor performance model. Based on these results, the LAPS flight unit will be capable of statically resolving hazards down to ~2 cm in depth and ~12 cm in width at 250 meters. This performance meets the mission requirement to detect hazards of 30 cm or larger (Table 1) starting at that range.

A companion paper describes the hardware-in-the-loop facility recently commissioned for testing motion compensation and safe site search in a dynamic environment at TRL-4/5 [12]. In the near future, the facility will be used to perform dynamic validation of the topographic and fuel cost map generation. Velocity determination and absolute navigation algorithms (also referred to as Terrain Relative Navigation in the literature), critical for the development of pin-point landing capability, will also be tested using this facility.

Future missions, both manned and unmanned, will require safe and accurate landings [19][20][21] enabled by a safe site detection functionality. This mission critical element is being addressed by MDA, NGC Aerospace, and Optech through the LAPS technology development program.

## 6. ACKNOWLEDGMENTS

## 7. REFERENCES

[1] de Lafontaine, J., Neveu, D., Lebel, K., Tripp, J., Martin, E., Ulitsky, A., Carr, R., Janes, S., "Autonomous Hazard-Avoidance Landing on the Moon: Adaptation and Demonstration of the LAPS System", Proceedings of the International Lunar Conference, (2005)

[2] Savage, D., Cook-Anderson, G., "NASA Selects Investigations for Lunar Reconnaissance Orbiter", NASA News, December 22 (2004)

[3] Braun, R.D., Manning, R.M., "Mars Exploration Entry, Descent and Landing Challenges", IEEE Aerospace Conference, Big Sky, Montana, 1-18, (2006)

[4] Brand, T., Fuhrman, L., Geller, D., Hattis, P., Paschall, S., Tao, Y.C., "GN&C Technology Needed to Achieve Pinpoint Landing Accuracy at Mars", AIAA/AAS Astrodynamics Specialist Conference and Exhibit; Providence, RI, 1: 1-12 (2004)

[5] de Lafontaine, J., Neveu, D., Kron, A., Hamel, J-F., Allen, A., Richards, R., "An Overview of Some Canadian Capabilities in Planetary Landing Techniques", 13th CASI Conference on Astronautics, Montreal, Canada, 25-27 Apr. 2006

[6] de Lafontaine, J., Neveu, D., Lebel, K., "Autonomous Planetary Landing Using a LIDAR Sensor: The Closed-Loop Functions", Paper 166821, Proc. 6th International ESA Conference on Guidance, Navigation and Control Systems, Loutraki, Greece, 17-20 Oct. (2005)

[7] de Lafontaine, J., Neveu, D., Lebel, K., "Autonomous Planetary Landing: the Quartic Guidance Revisited", Proc. 14th AAS/AIAA Space Flight Mechanics Meeting, Maui, Hawaii, 8-12 Feb. (2004)

[8] de Lafontaine, J., Gueye, O., "Autonomous Planetary Landing Using a LIDAR Sensor: the Navigation Function", Space Technology, 24(1) (2004)

[9] Lebel, K., Neveu, D., Lemay, C-E., de Lafontaine, J., Brunet C-A., "Laboratory Demonstration Of Fuel Optimal Hazard Avoidance Techniques For Autonomous Planetary Landing", Paper AAS 05-145, Proc. AAS/AIAA Space Flight Mechanics Meeting, Copper Mountain, USA, 23-27 Jan. (2005)

[10] Cheng, Y., Goguen, J., Johnson, A.E., Leger, C., Matthies, L., San Martin, M., Willson, R., "The Mars Exploration Rovers Descent Image Motion Estimation System", Intelligent Systems, 19(3): 13-21 (2004)

[11] Pollard, B.D., Sadowy, G., "Next Generation Millimeter-wave Radar for Safe Planetary Landing", Proceedings 2005 IEEE Aerospace Conference, 1213-1219 (2005)

[12] Langley, C., Yang, G., Mukherji, R., Taylor, A., de Lafontaine, J., Neveu, D., Lebel, K., Lemay, C-E., Richards, R., Tripp, J., Giroud, C., "Recent Advancements of the Lidar-based Autonomous Planetary Landing System (LAPS)", Proc. International Astronautical Conference, IAC-07-A5.2 (2007)

[13] "NSSDC Master Catalog Display: Spacecraft Viking 1 Lander" http://nssdc.gsfc.nasa.gov/database/MasterCatalog?sc=1975-075C, accessed June 11, 2007

[14] Hamel, J-F., Neveu, D., de Lafontaine, J., "Feature Matching Navigation Techniques for Lidar-Based Planetary Exploration", Proc. AIAA Guidance, Navigation and Control Conference, Keystone, Colorado, USA, 21-24 Aug. (2006)

[15] Jones EM, "Apollo Lunar Surface Journal", http://www.hq.nasa.gov/alsj/frame.html, accessed August 8, 2007

[16] de Lafontaine, J., Neveu, D., Hamel, J-F., Mukherji, R., Yang, G., Taylor, A., Giroud, C., "The LDTF: a Canadian Facility for the Validation of Hazard-Avoidance and Terrain-Relative Navigation for Planetary Landing", subject to acceptance at the CASI ASTRO 2008 Conference, Montreal, 28 April – 1 May 2008

[17] Pierrottet, D.F., Amzajerdian, F., Meadows, B.L., Estes, R., Noe, A.M., "Characterization of 3-D imaging lidar for hazard avoidance and autonomous landing on the Moon", Proc. of SPIE, 6550: 655008, (2007)

[18] Lichti, D.D., "New Angular Resolution Measure for 3-D Laser Scanners", Optical Engineering, 43(10): 2218-2219 (2004)

[19] Mattingly, R., Hayati, S., Udomkesmalee, G., "Technology development plans for the Mars Sample Return mission", IEEE Aerospace Conference, 982-995 (2005)

[20] Steigerwald, B., Stiles, L., "Proposed Mission Will Return Sample from Near-Earth Object", NASA News, March 9 (2007)

[21] Graham, J.B., "Prospecting Rovers for Lunar Exploration", IEEE Aerospace Conference, 1-11 (2007)